

# Charge transport properties of interstitially doped graphene: a first-principles study

Dwi Nugraheni Rositawati<sup>1,2</sup>, Moh. Adhib Ulil Absor<sup>1</sup>, Kuwat Triyana<sup>1</sup> and Iman Santoso<sup>1</sup>

<sup>1</sup> Department of Physics, Faculty of Mathematics and Natural Sciences (FMIPA), Universitas Gadjah Mada, Sekip Utara BLS 21, Yogyakarta 55281, Indonesia

<sup>2</sup> Department of Physics Education, Faculty of Teacher Training and Education, Sanata Dharma University, Jl. Affandi Mrican Tromol Pos 29 Yogyakarta 55002, Indonesia

E-mail: [iman.santoso@ugm.ac.id](mailto:iman.santoso@ugm.ac.id)

Received 10 March 2023

Accepted for publication 6 May 2023

Published 8 August 2023



CrossMark

## Abstract

The role of interstitial atomic doping on transport properties of graphene was systematically studied using first-principles density functional theory (DFT). The study revealed that interstitial Au doping results in a p-type transfer of holes to graphene as the dopant concentration increases to 25%, with the Dirac point shifting to the Fermi level and localised states of atomic dopants appearing at the Fermi level and at energy of  $-1$  eV. Ca, Ag and Al interstitial doping induces an n-type transfer of electrons to graphene with the Dirac point moving away from the Fermi level and localised states appearing at the Fermi level and at energy levels of  $\sim 2$  eV for Ca, around  $-3.5$  eV for Ag,  $-3.5$  eV and  $\sim 1.6$  eV for Al. As the dopant concentration increases further to 50%, the number of holes (or electrons) decreases for all dopants, except for Ca, as the localised state at the Fermi level disappears, and the Dirac point returns towards the Fermi level. Our research provides insights into how to reconcile the localised state and the number of charge carriers that play a significant role in the transport properties of interstitial doped graphene.

Keywords: graphene, interstitial doping, DFT, transport properties

Classification numbers: 3.02, 5.15

## 1. Introduction

Graphene is a 2D material with a thickness of 1 atom (0.335 nm) which is composed of carbon atoms bonded very tightly to form a hexagonal structure [1]. The experimental success in 2004 [2] has attracted great interest to carry out further experimental and theoretical research in condensed matter physics [3–6]. Its unique properties, such as high charge carrier mobility due to linear dispersion at the Dirac points, make it an excellent candidate for a wide range of electronic applications [2–8], optoelectronics [9], nanoelectronics [10], thermoelectric [11–17], sensors [18–20], energy conversion [21] and energy storage devices [22]. Due to its exceptional electrical, thermal, and mechanical properties [23, 24], including extraordinarily high carrier mobility [25, 26], thermal conductivity [27], and flexibility [28, 29], graphene has been suggested as a possible thermal management device. Although graphene has very high carrier

mobility, but its carrier concentration around the Fermi level is small [30, 31], thus limiting its application.

In order to maximise graphene potential, the electronic band structure of graphene around Fermi level must be modified to achieve higher charge concentration while keeping the linear dispersion. Previous studies shows that interstitial doping with various atoms will change the electronic structure of graphene [32] (e.g. Li, Ca, K, Al, Ga, In, Na, Ti, Sn, Pd [33], Fe [34], Au [33, 35], Ag, Cu [35], Mn [36]), in which its transport properties can be tuned in to n-type or to p-type graphene. In particular Au and Ag doping of graphene is broadly used as an electronic device [37–39] while Ca doping of graphene can exhibit superconductivity [40] and is widely developed as sensors [41], as well as Al-graphene used for plasmonic device [42]. However, the dopant concentration that is used for those application is either at very low concentration or becomes as a substrate. Although the doping process has increased the number of charge carriers in the pristine graphene, for particular dopant

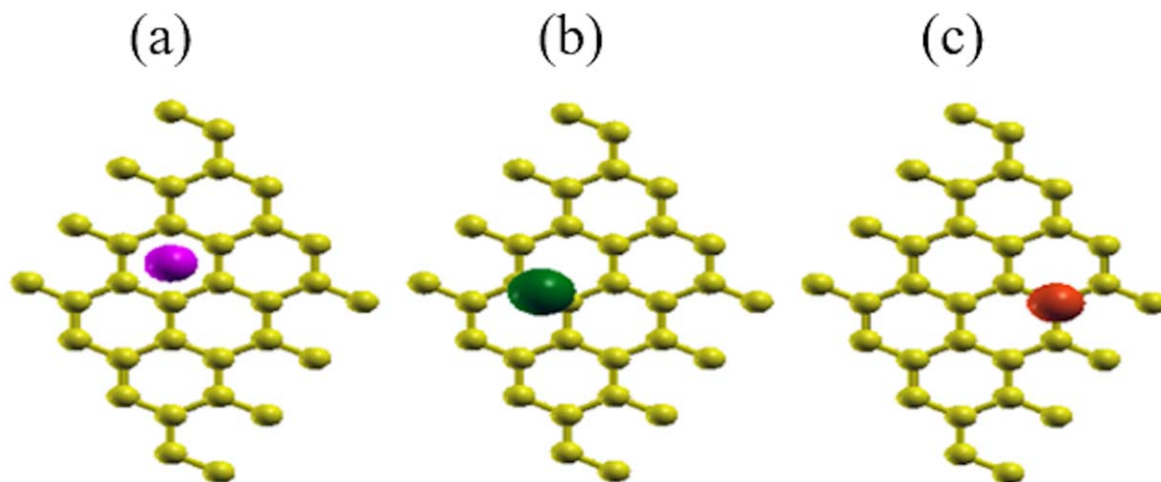


**Figure 1.** The three stable sites for doping on top view of the  $4 \times 4$  graphene supercell structure: (a) the hollow site (H) as shown by the purple sphere; (b) the bridge (B) as shown by the green sphere; and (c) the top (T) as shown by the orange sphere.

concentration its mobility seemingly shows different properties from pristine graphene which is indicated by the absence of linear dispersion around the Fermi energy [43]. Due to the interaction between atomic dopant and graphene during the doping process, the localised state will appear near the Fermi energy [44, 45]. If either of the above circumstances is dominant, it will cause a degradation in the transport properties (i.e. mobility and conductivity) of pristine graphene. Moreover, to measure the electronic transport properties of graphene, it is necessary to create connections with metal leads [46, 47]. Therefore, it is crucial to have a good understanding of the structural and electronic properties such as charge carriers between graphene and metal doping and distances between graphene and metal. The charge carriers between metal and graphene lead to doping of the graphene sheet. Depending on the type and amount of metal used, the doping can have different signs and magnitudes, allowing the connection of electrodes made of various metals to the graphene, enabling the formation of p-n junctions [48, 49]. Thus, it is interesting to study the role of the interstitial doping concentration on transport properties of graphene where the linear band condition persists.

This paper focuses on a systematic study of the interstitially doped graphene with various concentrations of Au, Ca, Ag, and Al atoms using first-principles density functional theory (DFT) calculations. Particular interest is to find the evolution of the electronic structure of the doped graphene since the controlling charge carrier on the graphene surface plays an important role in its electrical and thermal transport. This study is arranged as follows we explain the detail of computational methods in section 2. Then we give our findings together with thorough explanations, including the influence of interstitially doped graphene on its transport properties. Finally, in section 4, we review and conclude our results.

## 2. Computational methods

In this study, all calculations were done using the DFT [50–53], implemented in the OpenMX code [54], based on norm-conserving pseudopotential [55] and pseudo-atomic localised basis functions [56, 57]. The basis functions were expanded by linear combination of multiple pseudoatomic orbitals (PAO) generated using a confinement scheme [56, 57], where the accuracy of the basis functions as well as pseudopotentials (VPS) we used was carefully benchmarked by the delta gauge method [58]. The electronic exchange–correlation interactions are treated in the generalised gradient approximation (GGA) of Perdew–Burke–Ernzerhof [59]. The energy cut-off of 300 Ry was used and the energy convergence criterion was kept at  $1 \times 10^{-9}$  Hartree for each electronic structure calculation.

The graphene-doping systems were modelled using interstitial doping in the  $4 \times 4$  graphene supercell (made up of 32 C atoms), while the doping atoms were Au, Ca, Ag, and Al. In the z direction, a vacuum space of 25 Å was used in this study to avoid interlayer interactions. The doping atoms were arranged on three sites, namely the hollow (H) site at the center of the hexagon structure, the top (T) site just above the carbon atom, and the bridge (B) site at the center of the carbon–carbon bond (figure 1).

The effect of interstitial doping was studied by changing the dopant concentration from 3.125% (one dopant atom in 32 carbon atoms), 6.25% (two dopant atoms in 32 carbon atoms), 12.5% (four dopant atoms in 32 carbon atoms), 25% (eight dopant atoms in 32 carbon atoms), and 50% (sixteen dopant atoms in 32 carbon atoms). Geometry optimisation for T, H, and B sites was carried out for the 3.125% dopant concentration. The most stable site is chosen, which has the lowest total energy. For the 6.25% to 50% dopant concentration, geometry optimisation was carried out at the most stable site. The geometry of the pristine graphene supercell system and the graphene-doping systems was optimised in fully relaxed configurations until the Hellmann–Feynman force components acting on each atom were less than  $10^{-5}$

**Table 1.** Structural properties of Au, Ca, Ag, and Al doping at the top (T), hollow (H), and bridge sites (B) studied in this work. The properties listed are the number of dopant atoms on the supercell ( $N$ ); the distance between adjacent carbon atoms ( $d_{CC}$ ); the difference between the average of the  $z$  coordinates of the C atoms and the  $z$  coordinates of the adatom ( $h$ ); the distance between the adatom and its nearest carbon atom ( $d_{DC}$ ); total energy ( $E_{tot}$ ).

Dopant atoms	$N$	Doping concentration (%)	Site	$d_{CC}$ (Å)	$h$ (Å)	$d_{DC}$ (Å)	$E_{tot}$ (eV)
Au	1	3.125	T	1.43	2.90	2.90	-7957.346
	1	3.125	H	1.43	3.40	3.69	-7957.332
	1	3.125	B	1.43	3.12	3.20	-7957.344
	2	6.25	T	1.43	2.87	2.87	-10827.154
	4	12.5	T	1.43	3.47	3.47	-16567.379
	8	25	T	1.47	2.39	2.39	-28046.237
Ca	16	50	T	1.50	3.63	3.63	-51013.716
	1	3.125	T	1.43	2.50	2.50	-6100.622
	1	3.125	H	1.43	1.93	2.73	-6100.679
	1	3.125	B	1.43	2.47	2.57	-6100.608
	2	6.25	H	1.43	2.38	2.78	-7114.492
	4	12.5	H	1.43	2.39	2.78	-9142.684
Ag	8	25	H	1.50	2.19	2.65	-13188.338
	16	50	H	1.50	2.12	2.60	-21267.874
	1	3.125	T	1.43	3.29	3.29	-8190.391
	1	3.125	H	1.43	3.34	3.64	-8190.391
	1	3.125	B	1.43	3.32	3.40	-8190.392
	2	6.25	B	1.43	3.19	3.27	-11293.400
Al	4	12.5	B	1.20	2.72	2.79	-17484.173
	8	25	B	1.43	3.99	4.05	-29920.501
	16	50	B	1.43	4.40	4.46	-54760.510
	1	3.125	T	1.44	2.12	2.56	-5148.850
	1	3.125	H	1.44	2.12	2.56	-5148.850
	1	3.125	b	1.44	2.22	2.33	-5148.748
	2	6.25	B	1.44	2.34	2.55	-5209.743
	4	12.5	B	1.43	2.10	2.53	-5331.813
	8	25	B	1.50	2.63	3.02	-5577.762
	16	50	B	1.50	4.22	4.48	-6090.155

Hartree/Bohr. In particular, adatom positions are fixed at the  $x$ ,  $y$ -axes, and relaxed at the  $z$ -axis [33, 60, 61]. The values of doping height ( $h$ ), the C–C bond length ( $d_{CC}$ ), and the average of the carbon-doping atomic bond lengths ( $d_{DC}$ ) were determined from the optimised structures. The first Brillouin Zone was sampled using an  $8 \times 8 \times 1$  K-grid centered on the gamma ( $\Gamma$ ). The K-grid of  $12 \times 12 \times 12$  was employed for the calculation of the electronic density of states (DOS) and partial density of states (PDOS) for the graphene supercell structure.

### 3. Results and discussion

The unit cell of pristine graphene was found to have a lattice parameter of 2.47 Å, which is consistent with the previous results [32, 33, 62–64]. While the  $4 \times 4$  pristine graphene supercell structure was found to have a lattice parameter of 9.89 Å. This is very much consistent with the results of experiments [33, 62]. The  $d_{CC}$  of pristine graphene is 1.43 Å. Table 1 shows the effect of additional dopant atom on  $d_{CC}$ . Our calculations confirmed that  $d_{CC}$  will increase as the dopant atoms were added to graphene.

The optimisation of the graphene supercell structure with one dopant atom was done for each of the H, T, and B sites (figure 1). The results show that the total energies for the Ca doping are -6100.622, 6100.679 and -6100.608 eV for the T, H, and B sites, respectively, indicating that Ca doping has the most stable site at the H site. These findings are consistent with the previous results [60]. Similarly, Al doping also has the most stable site at the H site [33, 60] with a total energy of -5148.850 eV. In contrast, Au doping has the most stable site at the T site [32, 60] with a total energy of -7957.346 eV. Differently, Ag doping [32] (the total energy is -8190.392 eV) has the most stable site at the B site. Moreover, the effect of interstitial doping was studied by changing the dopant concentration from 3.125% to 50%. In the formed structure, almost no distortion was found. The total energy decreases with an increasing doping concentration.

#### 3.1. Au-doped graphene

The top view of Au doped on the  $4 \times 4$  graphene supercell structure after optimisation was shown in figure 2(a). The stable sites for Au doping on the graphene layer are the T sites. Figure 2(b) shows the result of band structure calculation for the Au-doped graphene supercell system. Au

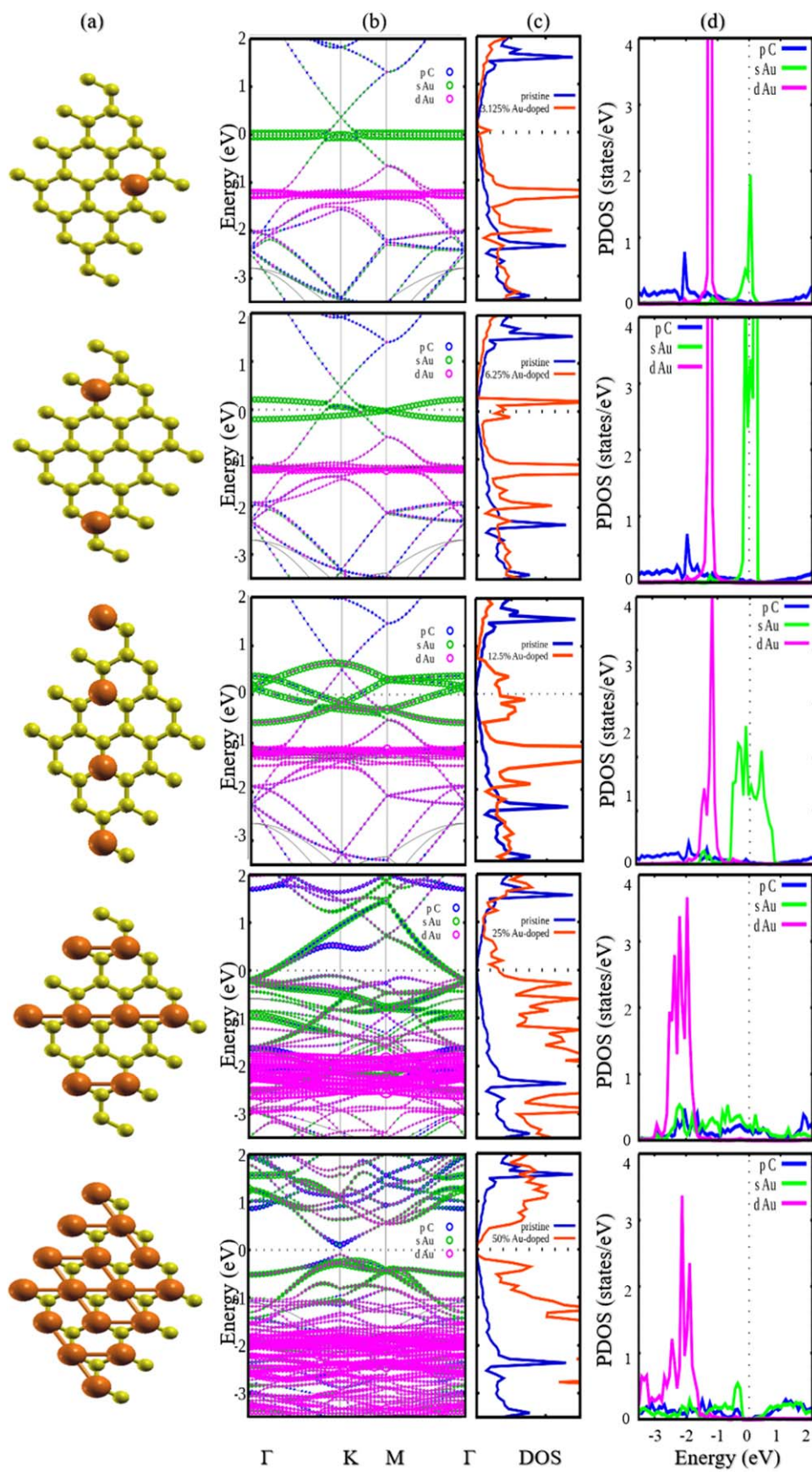


**Figure 2.** (a) Top view of Au doped on the  $4 \times 4$  graphene supercell structure after optimisation, (b) Projected band structure, (c) DOS, and (d) PDOS.

adsorption changes the band structure of graphene around the Dirac point (the Dirac point still lies at the K point) and shifts the Fermi level (the dashed lines), which is consistent with the DOS calculation (figure 2(c)). The calculated DOS confirmed that the graphene supercell system is a zero-gap semiconductor, which is in line with the previous results [1, 8, 65, 66]. The Fermi level shift in the Au-doped-graphene systems is due to the charge transfer from the graphene to the Au adatom [33], which is enhanced as the doping concentration increased. We find that the shifting of the Fermi level is at 0.4008 eV, 0.4810 eV, and 0.5611 eV below the Dirac point for 3.125%, 6.25%, and 12.5% Au-doped graphene, respectively, indicating that Au-doped graphene is electron-deficient. This implies that graphene with Au doping has the p-type character of charge carrier, which is in agreement with previous works [22, 23].

Interstitial Au doping on graphene also produces localised states at the Fermi energy and at energy levels of around  $-1$  eV for 3.125%, 6.25%, and 12.5% Au-doped graphene, as can be seen in the DOS and PDOS data (figure 2(d)). From our calculation, the localised state at the Fermi energy and at  $-1$  eV is due to the  $6s$  orbital and  $5d$  orbital of Au, respectively. When the concentration of Au atoms becomes 25%, the localised state at the Fermi energy disappears. The state at the Fermi level for this concentration is then equally determined by the  $s$  orbital of the Au atom and the  $p$  orbital of the C atom. At 50% of the Au concentration, the state at the Fermi energy further decreases, which may lead to the poorer transport properties. Moreover, the band dispersion close to the Dirac point changes to quadratic shape, suggesting that the electron gains more mass at this particular Au concentration.

### 3.2. Ca-doped graphene

The top view of Ca doped on the  $4 \times 4$  graphene supercell structure after optimisation was shown in figure 3(a). The stable sites for Ca doping on the graphene layer are the H sites. Figure 3(b) shows the result of band structure calculation for the Ca-doped graphene supercell system. Ca adsorption changes the band structure of graphene near the Dirac point. The increasing doping concentration causes an increase in the Fermi level shift in the band structure of graphene. This is in agreement with the results of DOS calculation (figure 3(c)). The DOS of the Ca-doped graphene supercell shows that the Ca doping changes the DOS near the Fermi level significantly. The Fermi level is observed to be shifted due to the charge transfer from the Ca adatom to graphene [33]. For graphene that is 3.125, 6.25, 12.5, 25, and 50% Ca-doped, the Fermi level shifting is at 0.8818 eV, 1.2224 eV, 1.3627 eV, 1.6834 eV, and 2.8858 eV above the Dirac point, respectively. The fact that Dirac point moves away from Fermi level as graphene is doped by Ca atoms indicates the electron-surplus nature of the Ca-doped graphene. This suggests the n-type charge carrier property of Ca-doped graphene, which is consistent with earlier works [32, 33].

Interstitial Ca doping on graphene also produces localised states at the Fermi energy and at energy levels of 2 eV for 3.125% and 6.25% Ca-doped graphene, as can be seen in the DOS and PDOS data (figure 3(d)). From our calculation, the localised state at the Fermi energy and at 2 eV is due to the  $4s$  orbital and  $3d$  orbital of Ca, respectively. When the concentration of Ca atoms becomes 12.5%, the localised state at the Fermi energy disappears while it still exists at 2 eV. Moreover, at 25% and 50% of Ca concentrations, the localised state at the Fermi energy also disappears and the localised state at 2 eV shifts to 0.5 eV. The fact that DOS decreased as the doping concentration rose might indicate that the Ca-doped graphene's transport characteristics deteriorated.

### 3.3. Ag-doped graphene

Figure 4(a) shows the top view of Ag doped on the  $4 \times 4$  graphene supercell structure after optimisation. The stable sites for Ag doping on the graphene layer are the B sites. Figure 4(b) shows the result of band structure calculation for the Ag-doped graphene supercell system. The Ag adsorption alters the band structure of graphene near the Dirac point. This is following the DOS of the Ag-doped supercell graphene (figure 4(c)). The charge transfer from the adatom to graphene results in the Fermi level shift [33]. The shifting of the Fermi level is at 0.1603 eV and 0.2405 eV above the Dirac point at 3.125% and 6.25% Ag-doped graphene, respectively. The Ag-doped graphene is electron surplus, implying that Ag-doped graphene has n-type character of charge carrier, which is consistent with previous study [32].

Interstitial Ag doping on graphene also yields localised states at the Fermi energy and at energy levels of  $-3$  eV for 3.125% and 6.25% Ag-doped graphene, as can be seen in the DOS and PDOS data (see figure 4(d)). From our calculation, the localised state at the Fermi energy and at around  $-3.5$  eV is due to the  $5s$  orbital and  $4d$  orbital of Ag, respectively. As for 12.5%, 25%, and 50% Ag-doped graphene, the localised state at the Fermi energy decreases while that at  $-3.5$  eV is still visible.

### 3.4. Al-doped graphene

The top view of Al doped on the  $4 \times 4$  graphene supercell structure after optimisation is shown in figure 5(a). The stable sites for Al doping on the graphene layer are the H sites. The results of band structure calculations for the Al-doped graphene supercell system are shown in figure 5(b). Al adsorption changes the band structure of graphene near the Dirac point. There is the Fermi level shift due to the influence of doping concentrations on graphene, which is consistent with the DOS calculation results.

Figure 5(c) shows the DOS of the Al-doped graphene supercell. The charge transfer from the adatom to graphene results in the Fermi level shift [33]. The Fermi level shift increases with increasing doping concentration. The shifting of Fermi level is at 0.8818 eV, 1.2024 eV, and 1.4429 eV above the Dirac point for 3.125%, 6.25%, and 12.5% Al-

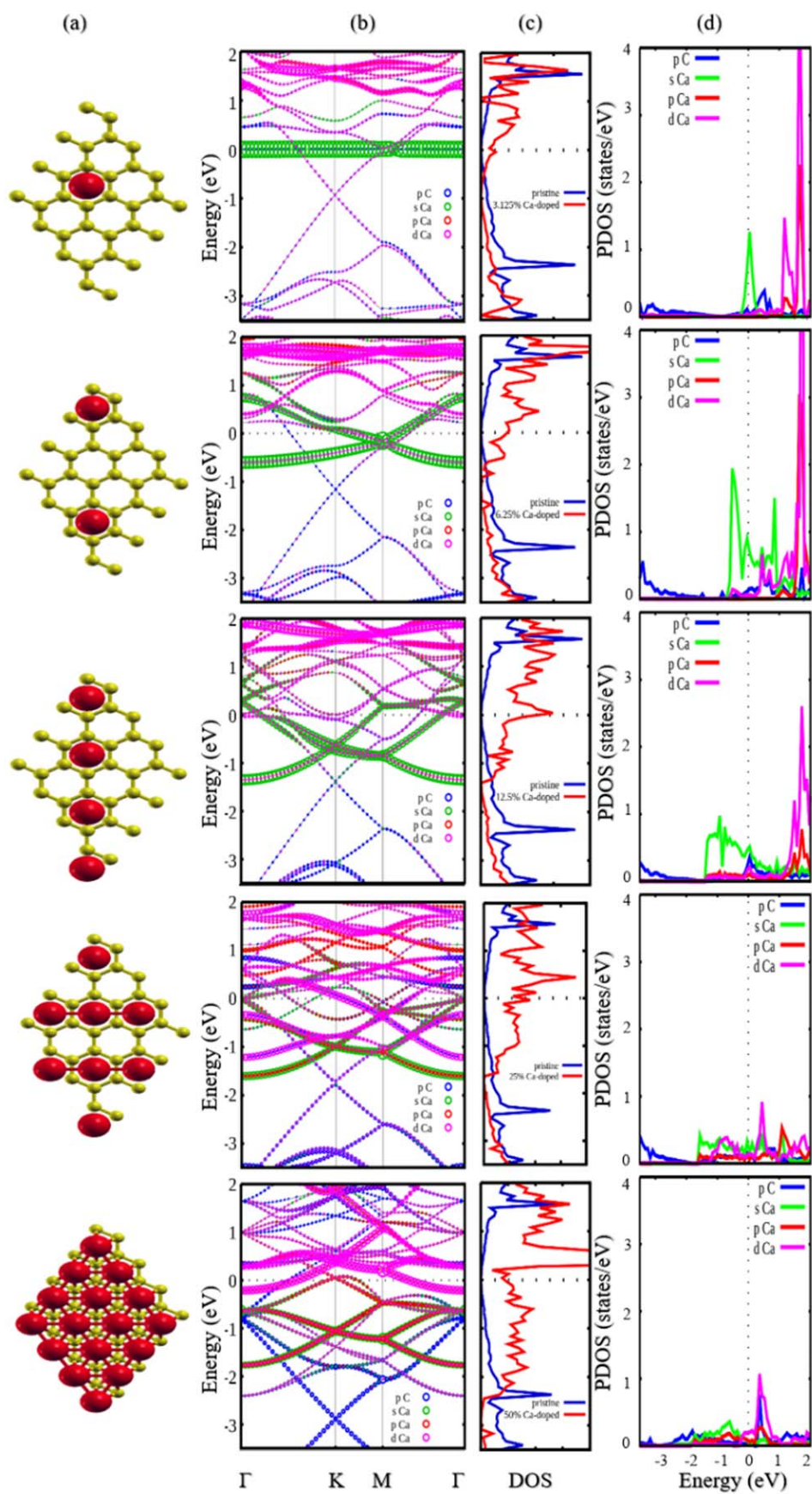


**Figure 3.** (a) Top view of Ca doped on the  $4 \times 4$  graphene supercell structure after optimisation, (b) Projected band structure, (c) DOS, and (d) PDOS.

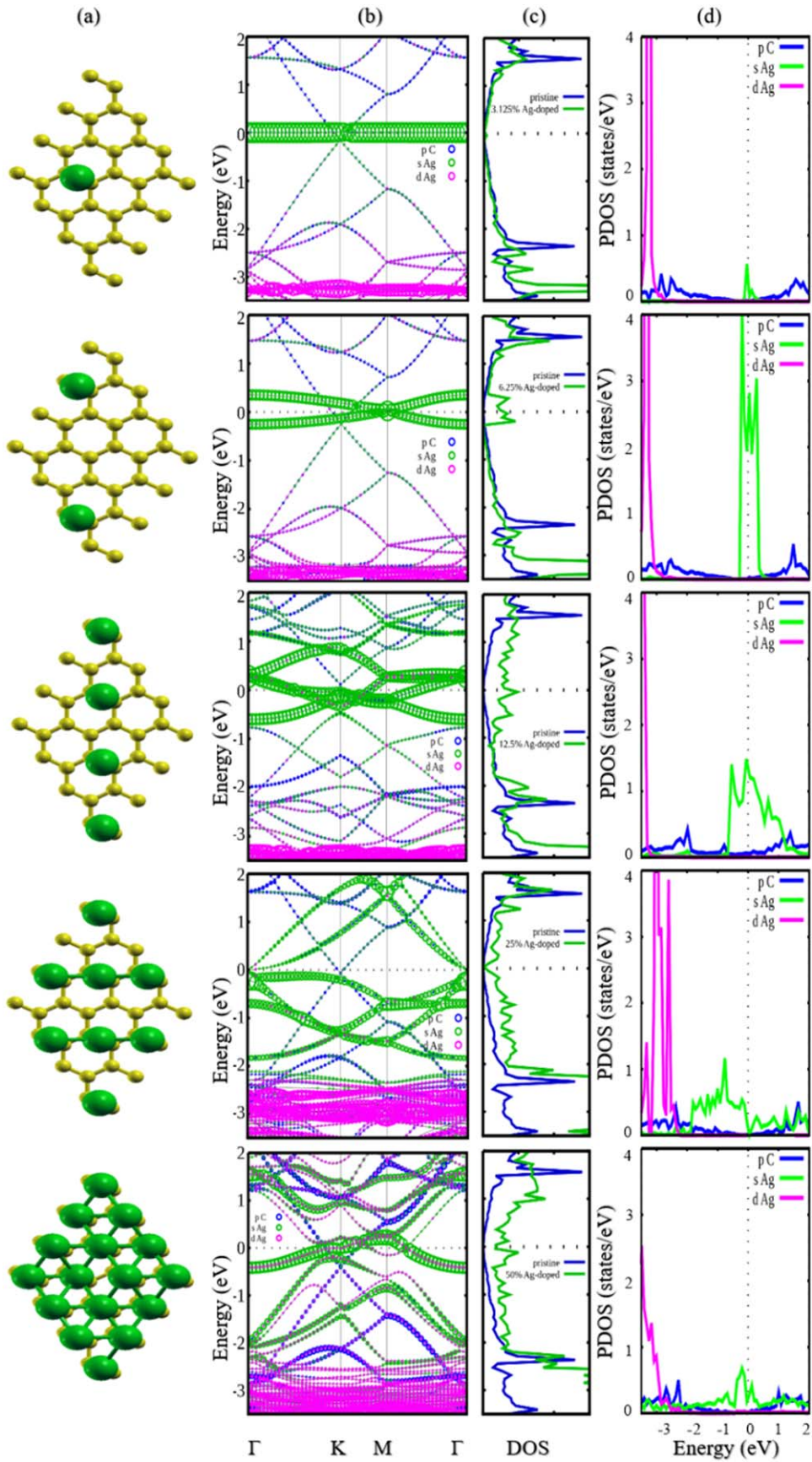


**Figure 4.** (a) Top view of Ag doped on the  $4 \times 4$  graphene supercell structure after optimisation, (b) Projected band structure, (c) DOS, and (d) PDOS.

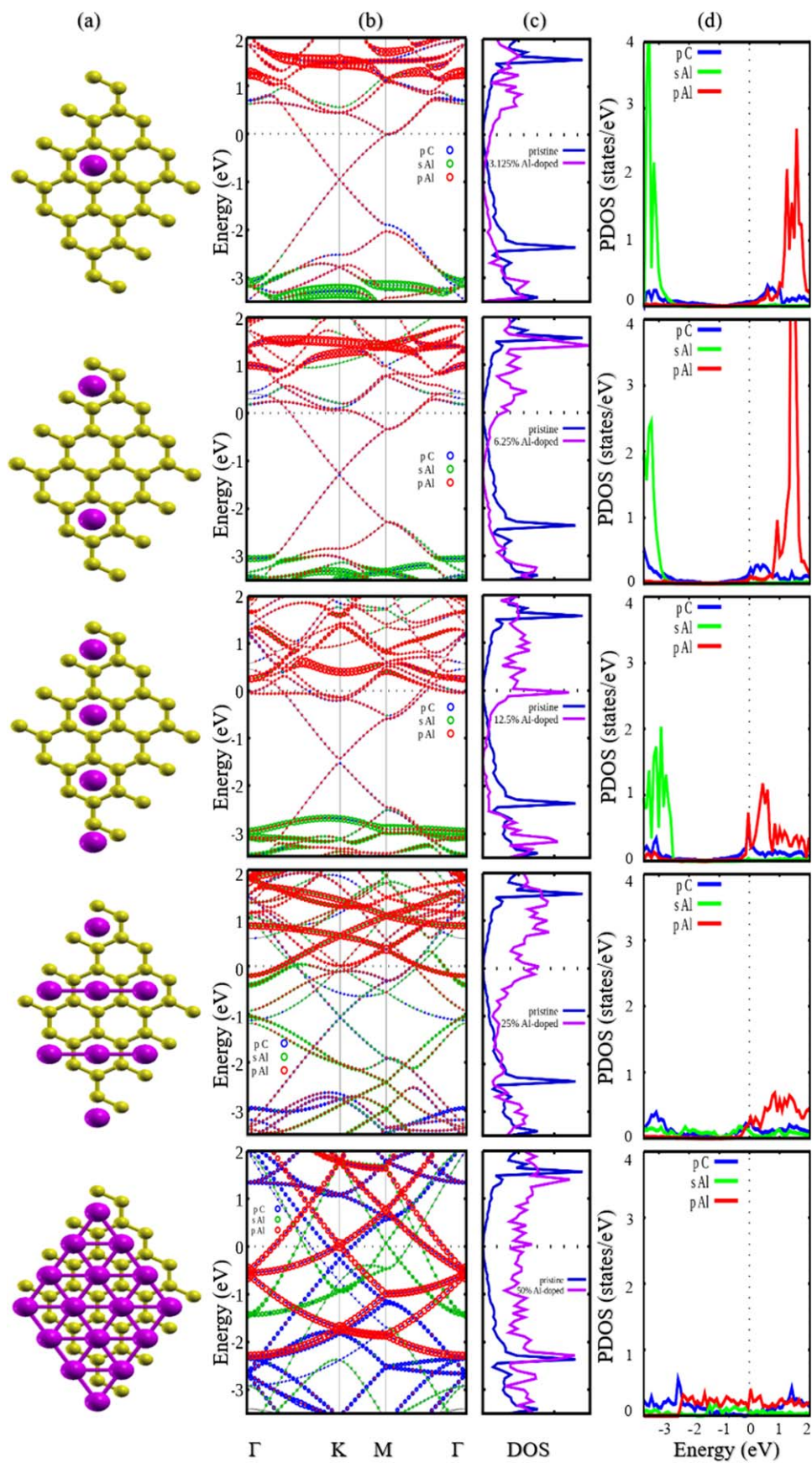


**Figure 5.** (a) Top view of Al doped on the  $4 \times 4$  graphene supercell structure after optimisation, (b) Projected band structure, (c) DOS, and (d) PDOS.

doped graphene, respectively. The Al-doped graphene is electron-surplus, implying that graphene with Al doping produces n-type graphene.

Figure 5(d) shows the partial density of states (PDOS) for Al and C atoms in the Al-doped graphene system for doping concentrations of 3.125%, 6.25%, 12.5%, 25%, and 50%. Interstitial Al doping on graphene also produces localised states at energy levels of around  $-3.5$  eV and at  $\sim 1.6$  eV for 3.125% and 6.25% Al-doped graphene. From our calculation, the localised state at energy levels of  $-3.5$  eV and at 1.6 eV is due to the  $3s$  orbital and  $3p$  orbital of Al, respectively. For 12.5% Al-doped graphene, the localised state seems to have decreased while at 25% and 50% Al concentrations, the localised state disappears and is replaced by broader states.

The presence of localised states at the Fermi level induced by Au, Ca, Ag, and Al interstitial doping can deteriorate the electrical transport properties of graphene. This is because the Fermi level is an energy level at which electronic states are most likely to be occupied, and any localised states at this level can act as trapping centers for charge carriers, leading to scattering and reduced mobility of charge carriers. Additionally, if these localised states are not fully occupied or empty, they can introduce additional impurity levels in the bandgap of graphene, further affecting its electrical properties. Therefore, the presence of localised states at the Fermi level can hinder the performance of graphene-based electronic devices, which rely on the high electron mobility of graphene [28, 67–69].

### 3.5. Charge transfer at linear dispersion regime

To further elucidate the interplay between the interstitial doping induced localised state and the linearity of graphene's band near K point, we will analyse the charge transfer that is extracted from band dispersion. The charge transfer from the adatom to graphene results in the shifting of the Fermi level [33]. Au doping on graphene shifts the Fermi level below the Dirac point. The position of the Dirac point ( $E_D$ ) increases with increasing Au doping concentration. On the other hand,  $E_D$  will decrease with increasing Ca, Ag, and Al doping concentrations. Ca, Ag, and Al doping shifts the Fermi level above the Dirac point. The charge transfer induced the shifting of Dirac cone around the Fermi level which may be caused by the difference of work function between graphene and atomic dopant [70] and by the electron affinity of atomic dopant [71].

Based on the assumption of linear dispersion of the DOS near the Dirac point, the concentration of charge carriers (electrons or holes) of doped graphene can be determined using equation (1) [70]:

$$N_e(N_h) = \frac{1}{\pi(\hbar v_F)^2} (|E_F - E_D|)^2, \quad (1)$$

where  $v_F \approx 10^6$  m/s is the Fermi velocity of graphene,  $E_F(E_D)$  is the energy position of the Fermi level (Dirac point).

According to figure 6, the concentration of charge carriers (holes) in graphene that is interstitially doped with Au, as determined by equation (1), rises as the concentration of Au

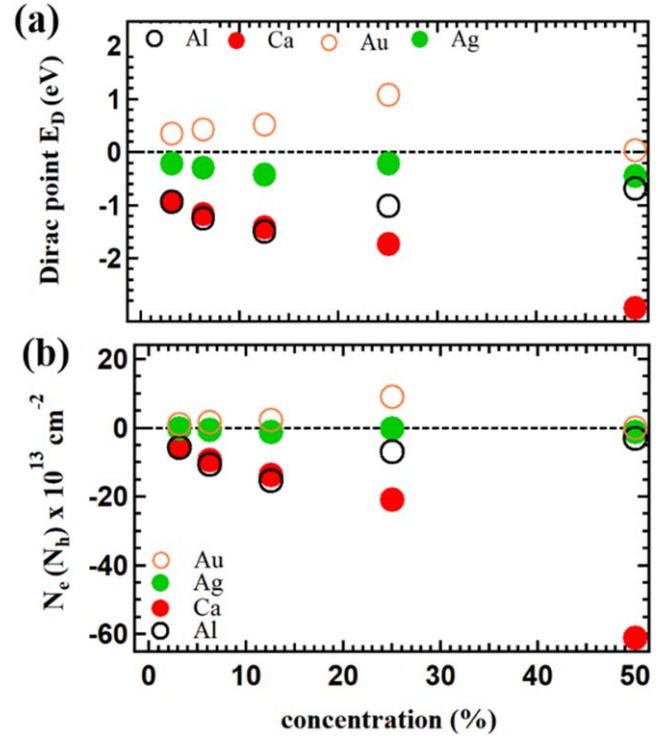


**Figure 6.** (a) Position of the Dirac point  $E_D$  at various concentrations of Au, Ca, Ag, Al-doped graphene, (b) Charge carrier density as a function of Au, Ca, Ag, Al doped graphene at linear dispersion regime.

doping increases up to 25%, but falls as the concentration increases to 50%. This may be due to the stronger presence of a localised state at  $-2$  eV (lower panel of figure 2(d)), which pushes the Dirac point towards the Fermi level. Au doping acts as p-type doping, leading to electron transfer from the graphene layer to the adatoms. The data presented in figure 6 also indicate that for Ca, Ag, and Al-doped graphene, the concentration of charge carriers (i.e., electrons) increases as the doping concentration increases up to 12.5%, with the exception of Ca, for which the concentration continues to increase until the Ca-dopant concentration reaches 50%. As the dopant concentration increases to 50%, the concentration of electrons in Ag and Al-doped graphene decreases even more. This could be explained by the presence of localised states at  $-3$  eV (in the case of Ag) and broader states around  $0 \div 2$  eV (in the case of Al), which can push the Dirac point closer to the Fermi level. The n-type doping provides electron transfer from the adatoms to the graphene layer.

## 4. Conclusions

To summarise, this study used DFT to investigate the electronic structure of graphene doped with interstitial Au, Ca, Ag, and Al. The study found that interstitial Au doping causes the Dirac point to shift to the Fermi level and localised states of atomic dopants to appear at the Fermi level and  $-1$  eV, resulting in a p-type transfer of holes to graphene as the dopant concentration increases up to 25%. Ca, Ag and Al

interstitial doping shifts the Dirac point away from the Fermi level and results in localised states of atomic dopants appearing at the Fermi level and at energy levels of  $\sim 2$  eV for Ca, around  $-3.5$  eV for Ag,  $-3.5$  eV and  $\sim 1.6$  eV for Al doping. This leads to an n-type transfer of electrons to graphene as the dopant concentration increases up to 12.5%. As the dopant concentration increased to 50%, the number of holes (or electrons) decreased for all dopants, except for Ca. This was caused by the disappearance of localised state at the Fermi level, leading to the Dirac point moving back towards the Fermi level. Our research offers an understanding of how to bring together the localised state and the number of charge carriers that are significant in the transport characteristics of graphene doped with interstitial atoms.

## Acknowledgments

The authors would like to thank UGM for providing financial support through Hibah Rekognisi Tugas Akhir (RTA) 2021 (No. 3143/UN1.P.III/DIT-LIT/PT/2021) and BPPDN 2019 Scholarship from Kemdikbud Indonesia.

## References

- [1] Castro Neto A H, Guinea F, Peres N M R, Novoselov K S and Geim A K 2009 *Rev. Mod. Phys.* **81** 109
- [2] Novoselov K S, Geim A K, Morozov S V and Jiang D 2004 *Science* **306** 666
- [3] Avouris P and Dimitrakopoulos C 2012 *Material Today* **15** 86
- [4] Xu Y, Li Z and Duan W 2014 *Small* **10** 2182
- [5] Fenta A S et al 2021 *J. Phys. Mater.* **4** 015002
- [6] Manadé M, Viñes F and Illas F 2015 *Carbon* **95** 525
- [7] Geim A K and Novoselov K S 2007 *Nature Mater.* **6** 183
- [8] Geim A K 2009 *Science* **324** 1530
- [9] Zheng Q, Li Z, Yang J and Kim J K 2014 *Prog. Mater. Sci.* **64** 200
- [10] An X and Yu J C 2011 *RSC Adv.* **1** 1426
- [11] Hao L and Lee T K 2010 *Phys. Rev. B* **81** 165445
- [12] Jafari A, Ramezani A H, Fayaz V and Hossienkhani H 2019 *Can. J. Phys.* **97** 1027
- [13] D'Souza R and Mukherjee S 2016 *J. Phys. Conf. Ser.* **759** 012040
- [14] D'Souza R and Mukherjee S 2017 *Phys. Rev. B* **95** 085435
- [15] D'Souza R 2018 and Mukherjee J. *Appl. Phys.* **124** 124301
- [16] Briones-Torres J A, Pérez-Álvarez R, Molina-Valdovinos S and Rodríguez-Vargas I 2021 *Sci. Rep.* **11** 13872
- [17] Hossain M S, Huynh D H, Nguyen P D, Jiang L, Nguyen T C, Al-Dirini F, Hossain F M and Skafidas E 2016 *J. Appl. Phys.* **119** 125106
- [18] Devi P K and Singh K K 2023 *Biosensors and Bioelectronics: X* **13** 100287
- [19] Jiaa X, Zhang H, Zhang Z and An L 2020 *Mater. Chem. Phys.* **249** 123114
- [20] Basu S and Hazra S K 2017 *Journal of Carbon Research* **3** 29
- [21] Lim S P, Pandikumar A, Huang N M and Lim H N 2015 *Int. J. Energ. Res.* **39** 812
- [22] Mao M, Hu J and Liu H 2015 *Int. J. Energ. Res.* **39** 727
- [23] Vining C B 2009 *Nat. Mater.* **8** 83
- [24] Dey A, Bajpai O P, Sikder A K, Chattopadhyay S and Khan M A S 2016 *Renew. Sustain. Energy Rev.* **53** 653
- [25] Bolotin K I, Sikes K J, Jiang Z, Klima M, Fudenberg G, Hone J, Kim P and Stormer H L 2008 *Solid State Commun.* **146** 351
- [26] Banszerus L, Schmitz M, Engels S, Dauber J, Oellers M, Haupt F, Watanabe K, Taniguchi T, Beschoten B and Stampfer C 2015 *Sci. Adv.* **1** e1500222
- [27] Balandin A A, Ghosh S, Bao W, Calizo I, Teweldebrhan D, Miao F and Lau C N 2008 *Nano Lett.* **8** 902
- [28] Kim K S, Zhao Y, Jang H, Lee S Y, Kim J M, Kim K S, Ahn J H, Kim P, Choi J Y and Hong B H 2009 *Nature* **457** 706
- [29] Jang H, Park Y J, Chen X, Das T, Kim M S and Ahn J H 2016 *Adv. Mater.* **28** 4184
- [30] De S and Coleman J N 2010 *ACS Nano* **4** 2713
- [31] Lu H, Guo Y and Robertson J 2017 *J. Appl. Phys.* **121** 224304
- [32] Tang Y, Yang Z and Dai X 2011 *J. Magn. Magn. Mater.* **323** 2441
- [33] Chan K T, Neaton J B and Cohen M L 2008 *Phys. Rev. B* **77** 235430
- [34] Mao Y, Yuan J and Zhong J 2008 *J. Phys. Condens. Matter* **20** 115209
- [35] Amft M, Lebegue S, Eriksson O and Skorodumova N V 2011 *J. Phys. Condens. Matter* **23** 395001
- [36] Mao Y and Zhong J 2008 *Nanotechnology* **19** 205708
- [37] Idisi D O, Oke J A and Bello I T 2021 *Int. J. Energy Res.* **45** 19772
- [38] Rohizat N S, Ripain A H A, Lim C S, Tan C L and Zakaria R 2021 *Sci. Rep.* **11** 19688
- [39] Rohizat N S, Ismail M N S M, Fahri M A S A, Tan C L and Zakaria R 2023 *Photonic Sens.* **13** 230307
- [40] Kotsakidis J C et al 2020 *Chem. Mater.* **32** 6464
- [41] Zhang R, Hao T, Hu S, Wang K, Ren S, Tian Z and Jia Y 2023 *Sensors* **23** 353
- [42] Shukla S and Arora P 2022 *Optik* **261** 169177
- [43] Joucken F et al 2015 *Sci. Rep.* **5** 14564
- [44] Tison Y et al 2015 *ACS Nano* **9** 670
- [45] Joucken F et al 2012 *Phys. Rev. B* **85** 161408
- [46] Schomerus H 2007 *Phys. Rev. B* **76** 045433
- [47] Huard B, Stander N, Sulpizio J A and Goldhaber-Gordon D 2008 *Phys. Rev.* **78** 121402
- [48] Fogler M M, Novikov D S, Glazman L I and Shklovskii B I 2008 *Phys. Rev. B* **77** 075420
- [49] Gorbachev R V, Mayorov A S, Savchenko A K, Horsell D W and Guinea F 2008 *Nano Lett.* **8** 1995
- [50] Hu W, Lin L, Yang C and Yang J 2014 *J. Chem. Phys.* **141** 214704
- [51] Parr R G and Yang W 1984 *J. Am. Chem. Soc.* **106** 4049
- [52] Hohenberg P and Kohn W 1964 *Phys. Rev.* **136** B864
- [53] Kohn W and Sham L J 1965 *Phys. Rev.* **140** A1133
- [54] Ozaki T et al 2020 User's Manual of OpenMX Ver. 3.9 (Tokyo), <https://openmx-square.org/>
- [55] Troullier N and Martins J L 1991 *Phys. Rev. B* **43** 1993
- [56] Ozaki T 2003 *Phys. Rev. B* **67** 155108
- [57] Ozaki T and Kino H 2004 *Phys. Rev. B* **69** 195113
- [58] Lejaeghere K et al 2016 *Science* **351** aad3000
- [59] Perdew J P, Burke K and Ernzerhof M 1996 *Phys. Rev. Lett.* **77** 3865
- [60] Nakada K and Ishii A 2011 *Solid State Commun.* **151** 13
- [61] Semidey-Flecha L, Teng D, Habenicht B F, Sholl D S and Xu Y 2013 *J. Chem. Phys.* **138** 184710
- [62] Lin X and Ni J 2012 *Phys. Rev. B* **86** 075440
- [63] Mapasha R E and Chetty N 2010 *Comput. Mater. Sci.* **49** 787
- [64] Garcia A L E, Baltazar S E, Romero A H, Robles J F P and Rubio A 2008 *Journal of Computational and Theoretical Nanoscience* **5** 2221
- [65] Ostad F Z, Ghazia M E, Javan M and Izadifarda M 2019 *Physica B* **575** 411678
- [66] Durajski A P, Auguscik A E and Szcześniak R 2020 *Physica E* **119** 113985

- [67] Chen J H, Jang C, Xiao S, Ishigami M and Fuhrer M S 2008 *Nat. Nanotechnol.* **3** 206–9
- [68] Liu L, Ryu S, Tomaschitz P, Regan W, Maultzsch J, Loh K P and Castro Neto A H 2011 *Nano Lett.* **11** 3112
- [69] Lherbier A and Charlier J C 2014 *Rep. Prog. Phys.* **77** 036502
- [70] Chen Z *et al* 2010 *Appl. Phys. Lett.* **96** 213104
- [71] Giertz I, Riedl C, Starke U, Ast C R and Kern C 2008 *Nano Lett.* **8** 4603